HHS Public Access

Author manuscript

Epilepsia. Author manuscript; available in PMC 2017 May 09.

Published in final edited form as:

Epilepsia. 2016 October ; 57(10): 1581–1593. doi:10.1111/epi.13501.

Continuous spike-waves during slow-wave sleep (CSWS) in a mouse model of focal cortical dysplasia (FCD)

Qian-Quan Sun[*], **Chen Zhou**, **Weiguo Yang**, and **Daniel Petrus**

Department of Zoology and Physiology, University of Wyoming, Laramie, WY 82071

Summary

Objective—To examine if mice with focal cortical dysplasia (FCD) develop spontaneous epileptic seizures and if so, what are the key EEG features.

Methods—Unilateral single freeze lesions to the S1 region (SFLS1R) were made in postnatal day 0–1 pups to induce a neocortical microgyrus in the right cortical hemisphere. Continuous 24-hour recordings with intracranial EEG electrodes and behavioral tests were performed in adult SFLS1R and sham-control mice to assess neurological status.

Results—A high percentage of adult SFLS1R animals (89%, 40/45) exhibited at least one or more spontaneous non-convulsive seizure events over the course of 24 hours. Of these animals, 60% (27/45) presented with a chronic seizure state that was persistent throughout the recording session, consisting of bursts of rhythmic high-amplitude spike-wave activities and primarily occurring during periods of slow-wave sleep. In comparison, none of the control, age-matched, mice (0/12) developed seizures. The epileptic discharge pattern closely resembled a pattern of continuous spike-waves during slow-wave sleep (CSWS) of the human syndrome described as an electrical status epilepticus during slow wave sleep (ESES). Key findings in the SFLS1R model indicated that the observed CSWS 1) were more prevalent in female (18/23) vs. male (9/22, $p < 0.05$), 2) were strongest in the right S1 region though generalized to other brain regions, 3) were associated with significant cognitive and behavioral deficits, 4) were temporarily alleviated by ethosuximide treatment or optogenetic activation of cortical GABAergic neurons, and 5) theta and alpha band rhythms may play a key role in the generalization of spike-wave activities.

Significance—This is the first report of an *in vivo* animal FCD model that induces chronic spontaneous electrographic brain seizures. Further characterization of the abnormal oscillations in this mouse model may lead to a better understanding of the mechanisms of CSWS/ESES.

[*]Correspondence should be addressed to: Dr. Qian-Quan Sun, 1000 E. University Ave, Dept. 3166, Laramie, WY 82071. Tel: 3072139688; neuron@uwyo.edu.

Author Contributions. QQS designed the experiments, performed data analysis and wrote the manuscript. CZ carried out the surgery, EEG recording and data analysis. WY performed neocortical freeze lesion and histological and physiological validation in brain slices. DP performed behavior experiments and behavior data analysis and wrote the behavior results.

Disclosure of Conflicts of Interest: None.

Ethical Publication Statement: we confirm that we have read the Journal's position on issues involved in ethical publication and affirm that this report is consistent with those guidelines.

There is supporting information with this article, including a supplemental table and a word document of extended online material and methods (with references).

Keywords

spike-wave seizure; cortical malformation; freeze lesion; optogenetic

Introduction

There are many human syndromes that are associated with focal cortical dysplasia (FCD) and malformations of cortical development (MCD), characterized by a disrupted architectural organization of the cerebral cortex[1]. MCDs are often highly correlated with pediatric epilepsy syndromes as well as cognitive disabilities, language problems, cerebral palsy and mental and psychiatric disorders. The incidence of medically intractable epilepsy that is associated with FCD has been increasingly documented and patients are often candidates for surgical intervention. However, many patients fail to achieve remission after surgery[1;2]. Therefore, the development of an animal model that mimics the clinical condition is of critical importance for understanding the underlying pathophysiological mechanisms and to test novel therapies of FCD/MCD related epilepsy[3].

A variety of injurious procedures applied to fetal brain *in utero*, or in new born pups, have been used to produce animal models of FCD[3;4]. These models mimic various aspects of the histo-pathology and neuronal hyper-excitability of clinical FCD/MCD and have been used to investigate the cause–effect relationships between FCD and epilepsy. A commonly used animal model of FCD, the rat neonatal freeze lesion, induces neuronal circuit abnormalities within cortical regions near the lesion that generate hyperexcitable discharges *in vitro,* even as the architectonic constituents of the focal region appears to be normal[5;6]. However, in this rat model, neither behavioral nor electrographic spontaneous seizures have been previously reported[7–9], despite highly reliable evoked epileptiform activity *in vitro*. Thus, it is unknown how the well-documented histopathological changes and hyperexcitability recorded *in vitro* leads to epilepsy or epileptogenesis *in vivo*.

Moreover, mismatches exist between epileptogenesis in animal models and human cases. In patients with MCD, intracranial electrophysiological recordings suggest large epileptogenic neural circuits that extend far beyond the limits of the detectable structural abnormality. Clinical cortical electrical stimulation and mapping studies have shown that malformed circuits are atypically organized and functionally abnormally integrated. However, current studies have yet to establish the relationship between the aberrant neural circuits and atypical organization associated with FCD with epileptogenesis *in vivo*. Therefore, the mechanisms underlying epileptogenesis associated with FCD remains elusive.

Our rational for creating a single freeze lesion in the somatosensory cortex was to evaluate whether a localized malformation to a defined thalamocortical circuit induces focal or generalized epileptiform activity *in vivo*. Therefore, we refer to our animal model as a single freeze lesion in the right S1 area (SFLS1R) to distinguish it from other, similar neocortical freeze lesion models, where broad S1 and sensorimotor areas were targeted[10;11]. Our data indicate that a majority of adult SFLS1R mice develop highly frequent repeatable spontaneous electrographic seizures that occur predominantly during slow-wave, non-rapid eye movement (NREM) sleep. The pattern of epileptiform discharges in these animals

closely resembles continuous spike-waves during slow-wave sleep (CSWS), which is a human epileptic syndrome associated with an EEG pattern of electrical status epilepticus during slow wave sleep[12–14], and clinically linked to Landau–Kleffner syndrome[15]. The mouse model reported here may potentially provide additional valuable insights into causality between FCD and CSWS and other translational research aimed at alleviating FCD related epilepsy.

Materials and Methods

The research procedures described herein were performed under protocols approved by the local IACUC. A more detailed version is available online as extended materials and methods. ***Animal procedure.*** Unilateral single freeze lesions were made in P0–1 mice pups (on a CD-1 or c57bl/6 background) to induce neocortical microgyria in the right S1 area (SFLS1R), as the author and colleagues previously described in rat[16]. Within a typical litter, both freeze lesion and sham (i.e. identical surgical procedures minus the freeze lesion) surgeries were performed. The entire litter was kept in a vivarium maintained at 22–23 °C on a normal 12:12 h light-dark cycle (lights on at 6:00 am). The mice were weaned and housed together based on the same sex. After EEG electrode implantation, all mice were singly housed in a dedicated room within the animal vivarium. ***Intracranial EEG recordings***. Mice were anesthetized under isoflurane anesthesia (2%, delivered in medical-grade oxygen) and secured in a stereotaxic frame. Polyimide-insulated stainless steel wires (0.005 inch, PlasticsOne, Roanoke, VA) and connecting pins (0.02 inch gold pins, Mill Max Manufacturing Corp, Oyster Bay, NY) were implanted as bipolar electrode pairs in several brain regions and secured in place with dental cement (e.g. Fig. 1A). A ground electrode was placed into the olfactory bulb area. A screw free, glue-based electrode assembly system that allows for long-term recordings was used for all EEG recording sessions (e.g. Fig. 1)[17]. A piezo-electric floor sensor was placed in the recording chamber to detect animal movement. EEG and floor-sensor signals were amplified via a differential AC amplifier (1–1000 Hz band pass filter), digitized at 100Hz, and recorded using Spike2 software (Cambridge Electronic Design). ***Power spectrum.*** Spectral power was performed using a FFT of the waveform data (3–20 seconds using 2.56-second Hanning window) across a continuous frequency range (0–50Hz) or conventional frequency bands (δ: 1–4 Hz, θ: 4–8 Hz, α: 8–12 Hz, σ: 12–16Hz and β: 16–24 Hz) for each electrode. ***Behavior***. All behavior testing was performed by an investigator blinded to the test group. We used a high-throughput automated home-cage behavior system, which provided an open field test, assessment of locomotion activities, social interactions, and repetitive behavior. The system automatically tracked animal activity (horizontal movement, rear-ups) level changes using a SmartCage™ automated platform (AfaSci, Menlo Park, CA) and data collected using CageCenter™ software across both light and dark cycles using 24 IR-sensors and a piezo-electric floor sensor. ***Optogenetic.*** We implanted a multi-mode fiber optic patch cable via a 1.25mm OD multimode ceramic zirconia ferrule (Precision Fiber Products, Inc, Milpitas, CA 95035), which was glued together with the S1R EEG electrode to form an optrode configuration. We implanted the optrode near the FL region in S1 of VGAT-ChR2 mice approximately 0.3mm below the skull. The multi-mode fiber optic patch cable was coupled to a blue laser. ***Ethosuximide***. Mice were anesthetized under isoflurane anesthesia (2%, delivered in

medical-grade oxygen). EEG recording wires were mounted first before ethosuximide (2 mg/0.5 ml distilled water[18]) was administered via i.p. injection. The mouse was then transferred to the recording arena for 24-hour EEG recordings. Sham-injected mice (saline only) was used as controls. ***Statistics.*** All values are expressed as mean ± SEM. Two-tailed Student's t test and ANOVA were performed on two or more group comparisons, respectively. A Kolmogorov-Smirnov test was used to determine parametric distribution of data. Paired t-tests were performed between on groups before and after ethosuximide treatment. Fisher's exact test were used to test sex differences. Significance was placed at $p < 0.05$. A more detailed methods section is available online from extended materials and methods section.

Results

The single focal cortical malformation was first validated in three month old mice (n=5). As shown in Figure 1, SFLS1R typically caused a single microgyrus in the S1 barrel field of the somatosensory cortex (Fig. 1B). The microgyrus, which is defined as having an altered lamination (Fig. 1B3), was found to be consistent with little variabilities in 5/5 mice and occupied around $0.2mm^2$ (0.4±0.1 mm in the medial-laterally direction and 0.5 ± 0.2mm in the rostral caudal directions respectively, n=5). This area represents around 5% of the size of mouse barrel field[19]. Majority of the mice included in this study are still being investigated and are thus unavailable for histological verifications.

1. Ictal-state in SFLS1R but not sham-treated animals

Shortly after EEG electrodes implantation (at variable age, see Supplemental Table S1 for details), continuous EEG recording was performed in 45 SFLS1R (10 ± 1 months old) and 12 sham-treated control adult mice (11 ± 2 months old). Typically, 2–3 pairs of bipolar EEG electrodes were implanted in S1R (typically in a more rostral location near the freeze lesion treated area, e.g. Fig. 1A), as well as other brain areas (e.g. contralateral S1, ipsilateral M1, and hippocampus). In sham-treated animals, EEG during sleep was dominated by slow-wave activity (i.e. NREM sleep) interspaced with brief movements (Fig. 2A1–3). δ-band activity was high during the NREM sleep period, compared with other sleep stages (Fig 2B2). Spindle waves, which peaked at around α band (8–12Hz), were usually very brief and interspersed among δ-band activities (Figs. 2A3 and B1 &3). Low amplitude REM activities interspersed between NREM activities (Fig 2A3 and B). Different sleep activities (REM, NREM, spindle) and wake activities showed distinct power spectra pattern (Fig 2B1 & 2).

SFLS1R mice exhibited similar δ-band activities that dominated the NREM sleep period (Fig. 3A1). In addition, spontaneous electrographic seizure activities were highly frequent during sleep. As demonstrated by the examples in Figure 3, 89% SFLS1R (i.e. 40 out of 45, Supplemental Table S1) and 0% sham-treated mice (n=12) exhibited spontaneous electrographic seizures, characterized by a barrage of prolonged (39 ± 2.6 seconds), high-voltage, negative and (or) positive rhythmic ictal-spikes recorded with intracranial EEG implants in the malformed area (S1R, Fig. 3A). The seizures were non-convulsive in nature as determined by long-term IR-video monitoring and lack of movement during ictal events (e.g. Fig. 3A2 see sensor signal during seizure). Spectral power analysis of the S1R EEG

signals indicated that the majority of the ictal-spike events resembled the generalized spike-wave discharges reported in GAERS rats [20] and other genetic mouse seizure models[21], with dominant frequencies in the α (8–12Hz) and θ (4–8Hz, Figs. 3B and 4A2) bands, and secondarily in higher frequency bands (>12Hz, Fig 3B and 4A2). In addition, there was a significant reduction in the δ-band power during seizure events (Fig. 3B2). The first ictal-spike (IS) events were usually detected at 5 months of age (n=4). In 4 mice, in which long-term recordings were performed, ictal spikes persisted after the initial discovery of ictal-spikes (average = 4.9±0.6 months), with little change in the power spectrum of the ictal-spikes. In all other animals, recordings were repeated at least once after 2–3 months, all ictal-spikes persisted in the following-up recordings. Over the course of these studies, 12/45 SFLS1R animals died of natural causes (average age = 16±2 months) as compared to 6/12 sham animals died of natural causes (average age = 20±2 months, p=0.21 between groups, Supplemental Table S1). There were no statistical differences in the estimated survival age between SFLS1R mice (21±1 months) and sham-treated mice (20±1 months, p=0.39), based on a by Kaplan-Meier analyses and log-rank tests. The locations of EEG implants were verified histologically. Within 45 SFLS1R mice, 23 were female and 22 were male (Supplemental Table S1). CSWS were present in 78% (18/23) female vs. 40% (9/22) male mice ($p<0.05$ between groups). Among 18 female animals exhibiting persistent chronic seizures, 5/8 were younger than 8 months (pre-menopausal group[22]), 9/10 were between 8–12 months, and 4/5 were older than 12 months of age (post-menopausal group[22]). Using Fisher's exact test, there were no statistical significance between pre vs. post-menopausal group (p=0.58). Thus we conclude that the occurrence of chronic seizure is unlikely to be directly affected by the ovarian cycle at the time of recording.

2. The relationship between CSWS and sleep-wake cycle in SFLS1R animals

Among the 40 SFLS1R mice exhibited spontaneous electrographic seizures, ictal-spikes in 13 mice were infrequent (i.e. less than 50 events over 24-hour period). 27 of the 45 SFLS1R mice (i.e. 60%) exhibited highly frequent, persistent and repeatable spontaneous electrographic seizures. Subsequent analysis of electrographic seizures was focused on these 27 animals. Ictal-spikes in these mice occurred spontaneously throughout the 24-hour recording period, typically showed a wax-and-wane formation (e.g. Figs. 3A2 and 4A1 &B2), and continued for tens of seconds or even several minutes (interrupted by brief movements or NREM sleep, Figs. 3A2 and 4B2). To further characterize the occurrence of the ictal-spikes during the natural sleep-wake cycle, sleep analysis (see extended methods) was performed in 6 SFLS1R mice and 4 age-matched sham controls. In these mice, ictal-spikes occurred during both quiet wake state as well as sleep, however, the ictal-spike activities are both much longer (276%, $p < 0.05$) and more frequent (178%, $p < 0.01$) in sleep vs. wake state. During the sleep state, the ictal-spikes exhibited a pattern of epileptiform activity closely resembling the clinical description of CSWS (Fig. 3A2 and 4B2). Indeed, further characterization of the CSWS in mice indicated a repetitive nature of the CSWS activity: 1) each CSWS event was composed of many repeating wax-and-wane spike-wave discharges; 2) the power-spectrum indicated a highly stereotypical pattern of repeating α (8–12 Hz) and θ (4–8 Hz) band activity (Figs. 4B3 and B4); 3) CSWS occurred predominately throughout the sleep-phase (Fig. 4B1), occupying 10–90% of total sleep time over the course of 24 hours (Fig 4B5) in different animals. In this cohort of animals, 5/6 of

the SFLS1R mice exhibited chronic CSWS, while none of the sham-treated animals (n = 4) exhibited EEG seizures at any period. We also examined the sleep structure of these animals. Compared with control animals, the SFLS1R mice showed a lower percentage of NREM sleep and similar amount of time in the wake-state (Figs. 4B6), thus the overall sleep-time and wake time are similar between sham and SFLS1R mice, although the sleep-structure was altered. Because REM sleep is defined by the higher θ (4–8 Hz) / δ (1–4 Hz) ratio, similar to ictal-spikes (e.g. Fig. 4A2), "REM-sleep" in SFLS1R mice represents a mix of both ictal-spikes and REM sleep. Thus we plotted the total percentage of REM and ictal-spikes together in sleep analysis and this portion activities constitute18.6% of total time (vs. only 9.1% in sham-treated animals, Fig. 4B6). Thus the overall increase in percentage of 'REM sleep' indicate potential occurance of ictal-activities during sleep. Nonetheless, the sleep structure correlated well with the light-dark cycle in both groups (e.g. Fig. 4B1), and no circadian deficits were detected.

3. Spatial propagation and correlation of the CSWS

Dual or triple EEG electrodes were implanted in 22 SFLS1R animals to examine temporal and spatial propagation of CSWS activities across the mouse brain. As shown in Figure 5(A–D), CSWS events were detected throughout the ipsilateral cortex (both sensory and motor regions), contralateral cortex, ipsilateral thalamus of SFLS1R animals, indicating that CSWS activity was highly generalized. To compare the degree of synchrony between different brain regions, we performed coherence and cross-correlation analysis between simultaneously recorded CSWS events. Our data indicate that CSWS recorded in the ipsilateral cortex, particularly between M1 and S1 region, has the highest degree of synchrony (Figs. 5A4 and E). Nonetheless, CSWS between S1R and ipsilateral VPM, contralateral S1 indicated varying degrees of synchrony as well (Figs. 5A4–B4 and E). Interestingly, synchronization of ictal-spikes between these remote brain regions were concentrated to α (8–12 Hz) and θ bands (4–8 Hz, Fig. 5A3–D3), suggesting that these lower frequencies are potentially involved in the generalization and synchronization across different brain regions.

4. CSWS modulation by ethosuximide administration or bilateral optogenetic cortical activation of GABAergic neurons

To further understand the properties of the CSWS activities in SFLS1R mice, we administered ethosuximide (2 mg/0.5 ml distilled water via i.p. injection), in 6 CSWS mice and performed 24-hour EEG recordings before and after the ethosuximide-treatment. Our data indicate that ethosuximide administration significantly prolonged the onset of CSWS (Fig. 6A3, n=6) and drastically reduced the total number of CSWS events over a 24-h period (Fig. 6A2, n=6). Because ethosuximide is the first choice anticonvulsant for absence seizures by suppressing thalamocortical network oscillations[23,24], our data further validate the spike-wave discharge nature of the spontaneous epileptiform activity in SFLS1R mice, and suggest the involvement of thalamocortical networks[25–27]. To probe the role of the cortical inhibitory networks in the CSWS, we implanted a fiber optic probe in the S1 region bilaterally in 5 SFLS1R mice, generated on an optogenetic background (VGAT-ChR2 mice), in which ChR2 is expressed in all GABAergic cells[28]. Once a CSWS event was detected (based on visual detection from the EEG record), we activated local cortical GABAergic cells by

applying 5 Hz blue laser stimulation to either the ipsilateral (S1R) or contralateral (S1L) side of the brain. Our results indicated that optogenetic stimulation, at either side (S1R or S1L), significantly attenuated CSWS activity during the time of laser stimulation, but CSWS events often resumed once the laser stimulation was stopped (Fig. 6B). The characteristic α (8–12 Hz) and θ (4–8 Hz) activity of the CSWS were also significantly attenuated during the 5-Hz laser stimulation (Fig. 6B4, n=3, *p< 0.05), similar results were seen with 10Hz stimulation but not 1Hz stimulation (data not shown). Taken together, these results suggest that cortical GABAergic networks play a crucial role in the continuation of CSWS and further support the idea that α (8–12 Hz) and θ (4–8 Hz) band activity plays a main role in generalization and propagation of spike-wave-discharge activity cross different brain regions.

5. CSWS is responsible for elevated cognitive and behavior changes

Because only 27/45 of animals exposed to a FCD developed frequent CSWS and around 10 animals had either no EEG seizures (n=5) or very low frequency ictal-spikes (n=13), we next examined whether CSWS activity alone caused any relevant changes in animal cognition or behavior by comparing behavioral outcome in a cohort of mice with similar FCDs but with (w/, n=20) and without (w/o, n=11) CSWS. We first examined if SFLS1R mice exhibited any sensory deficits by performing a gap-crossing test, a task that is dependent on the function of the whisker system[29]. We found that SFLS1R mice, performed similarly to sham-treated mice (gap distance d=7.3 ±0.7cm vs. d=7.2±0.5cm, n= 9, p>0.5), regardless whether they have seizure or not (table 1), Therefore, the SFLS1R mice did not exhibit major deficits in this whisker-dependent sensory task.

Open Field (OF) tests—SFLS1R mice w/CSWS seizures spent significantly less center time compared to SFLS1R mice w/o CSWS seizures (27% decreased, table 1). SFLS1R mice w/CSWS also had 10% decrease in active counts (table 1) and 17% decreased in total distance traveled vs. mice w/o CSWS seizures. These data indicate that SFLS1R mice with w/CSWS seizures are less exploratory and less active in mildly stressful conditions.

Social Interaction (SI) Test—SFLS1R mice w/CSWS seizures exhibited social interaction behavior that was significantly different from that of SFLS1R mice w/o CSWS seizures. SFLS1R mice w/CSWS seizures spent 20% more time with the stranger mouse compared to mice w/o CSWS seizures (table 1). SFLS1R mice w/seizures also had 15% increased active counts as compared to SFLS1R mice w/o seizures (p<0.05). These data suggest that SFLS1R mice w/CSWS seizures spend an abnormally longer-time socially interacting with the stranger mouse, indicative of a disinhibition towards the stranger mouse.

Novel Object Recognition (NOR) Test—SFLS1R mice w/CSWS seizures exhibited a similar distribution of time spent on examining novel vs. familiar objects as mice w/o CSWS seizures (table 1). However, SFLS1R mice w/CSWS seizures spent significantly more (52%) time with the both objects as compared to SFLS1R mice w/CSWS seizures (table 1). These data indicate that, although SFLS1R mice w/CSWS seizures were able to identify the novel object, it took them twice as long to complete the task suggestive of a cognitive deficit in these animals.

Discussion

Here, we report that a single neonatal freeze lesion to the somatosensory cortex induces a highly reproducible chronic epileptic condition characterized by the presence of CSWS. In previous animal studies, neither behavioral or electrographic seizures have been observed in neonatal freeze lesion models of FCD[7–9], despite highly reliable evoked epileptiform activity *in vitro.* Therefore this is the first demonstration of spontaneous seizure activity in vivo. In previous studies, EEG monitoring in animals exposed to FCD was performed at either early stages (2 months of age in the Kellinghaus study[8]), or in very short recording periods (20 min in the Scantlebury study[9]). In contrast, we made intracranial EEG implantations at ~4 months of age or older and continuously monitored EEG activities over 24 h at a frequency of once per week, a procedure that was recommended in a review[30]. Our data shows that SFLS1R mice developed a pattern of epileptiform discharges closely resembles CSWS, which in human cases is associated with ESES[12–14;31] and linked to Landau–Kleffner syndrome[15]. There are several similarities between the EEG features associated with clinical CSWS and related KLS and that recorded in our mouse model: 1) epileptic discharges are highly associated with sleep and are often manifested as typical spike-wave discharges; 2) epileptic encephalopathy with CSWS belongs to the group of focal-onset epilepsies, similarly CSWS in our SFLS1R mice was associated with a focal cortical malformation; 3) CSWS are associated with significant cognitive and behavior deficits.

There also appears to be some differences between our rodent model and the clinical condition. First, in clinical CSWS cases, remission generally occurs before adolescence even if most patients had persistent neuropsychological issues. In contrast, in our mouse model, CSWS were detected at the full adult stage and once detected, persisted throughout life based on data obtained so far. Second, clinical CSWS are not always associated with FCD/MCD, and the cause of ESES spectrum disorder is unclear. However, around 10% of patients with FCD/MCD show ESES. CSWS has also been reported in children with cerebral palsy showing brain lesions like polymicrogyria. We believe that these differences may stem from the fact that clinical CSWS is an epileptic spectrum disorder resulting from more complex pathological conditions, while FCD/MCD related clinical seizures are usually highly persistent. In addition, children suffer from CSWS often receive antiepileptic treatment, which could also account for the differences observed between human and mice.

In SFLS1R mice, CSWS are more frequent and longer lasting during sleep and have characteristics that implicate thalamocortical dysfunction. The mechanisms of epileptogenesis associated with clinical CSWS/ESES are still unclear. Results from this and previous studies from the rodent malformation models provide important insights. 1) In cortical slices obtained from freeze lesioned rats, evoked epileptiform activities can spread to almost the entire cortex[10]. 2) This effect is similar in S1 malformation models [16] or more wide-spread malformations exceeding S1[5]. 3) Nonetheless, an imbalance of excitation and inhibition has been widely documented in these models[5;11;32–39]. 4) Very interestingly, the impaired inhibition can be found quite distal from the malformation[40], even the contralateral side of the cortex[36]. These previous results from rat models may help understand the

mechanisms underlying epileptogenesis of CSWS, though data in the current mouse model is still lacking.

With regard to spike-wave discharges, several scholars have put forward a theoretical framework in which sleep spindles and generalized spike-wave discharges emerge from similar circuit mechanisms[25–27]. Based on this theory, circuitry that is present in the normal, non-injured brain likely exists as a 'template' upon which pathological changes are placed[25]. However, animal data supporting this theory is largely absent. Our data presented here support this idea, as indicated by the close association of spike-wave discharge with NREM-sleep and the generalized CSWS observed between cortex and thalamus. Thus, our mouse model potentially links FCD related chronic spontaneous ictogenesis with dynamic changes of circuits in the malformed brain *in vivo*. Our experiments using optogenetic manipulations and pharmacological modulations further support this idea: 1) the CSWS activities are suppressed by the first choice anticonvulsant for absence seizures[23,24]; 2) CSWS are inhibited by bilateral activation of cortical GABAergic networks. Sex and ovarian hormones (in rat) play a significant role in the modulation of induced paroxysmal seizure events such that females developed more frequent seizures[41]. Similarly in this study, CSWS were more frequent in females, presumably due to mechanisms similarly described in rats. Further investigation into these key questions may help to unravel the mechanisms by which normal circuits are transformed into epileptic circuits and help develop circuit-based treatment strategies for intractable epilepsies associated with CSWS/ESES, or FCDs/MCDs.

Behavior deficits similar to that observed in this study has also been reported in a chemical-induced models of cortical malformation[42]. Due to the more wide-spread malformations induced by the chemical treatment, it is unclear to what extent these deficits are due to structural changes or functional deficits that are caused by epileptic events. In the SFLS1R model, animals exhibiting CSWS had significant behavioral deficits as compared to freeze lesion animals without seizures. Thus our data highlight the contribution of electrographic seizures to the cause of these broad learning and cognitive deficits and suggest the idea that CSWS, presumably acting via broad effects on brain networks as well as sleep disturbances, may underlie the formation of distinct behavioral changes.

Supplementary Material

Refer to Web version on PubMed Central for supplementary material.

Acknowledgments

The research is support by grants from NINDS (No. 5R01NS094550 and 5R21NS084182) and NIGMS (P20GM103432). We thank Ms. Chunzhao Zhang and Lina Fan for providing technical assistance. We thank Dr. Anthony Williams for critical reading of the manuscript. We thank to Dr. Liang Zhang from University of Toronto, Western Research Institute for consultation with regard to the use of screw free EEG recording techniques.

Reference List

1. Schwartzkroin PA, Walsh CA. Cortical malformations and epilepsy. Ment Retard Dev Disabil Res Rev. 2000; 6:268–280. [PubMed: 11107192]
2. Cohen-Gadol AA, Ozduman K, Bronen RA, et al. Long-term outcome after epilepsy surgery for focal cortical dysplasia. J Neurosurg. 2004; 101:55–65. [PubMed: 15255252]

3. Luhmann HJ, Kilb W, Clusmann H. Malformations of cortical development and neocortical focus. Int Rev Neurobiol. 2014; 114:35–61. [PubMed: 25078498]

4. Dvorak K, Feit J. Migration of neuroblasts through partial necrosis of the cerebral cortex in newborn rats-contribution to the problems of morphological development and developmental period of cerebral microgyria. Histological and autoradiographical study. Acta Neuropathol. 1977; 38:203–212. [PubMed: 899721]

5. Jacobs KM, Kharazia VN, Prince DA. Mechanisms underlying epileptogenesis in cortical malformations. Epilepsy Res. 1999; 36:165–188. [PubMed: 10515164]

6. Redecker C, Hagemann G, Kohling R, et al. Optical imaging of epileptiform activity in experimentally induced cortical malformations. Exp Neurol. 2005; 192:288–298. [PubMed: 15755546]

7. Gibbs SA, Scantlebury MH, Awad P, et al. Hippocampal atrophy and abnormal brain development following a prolonged hyperthermic seizure in the immature rat with a focal neocortical lesion. Neurobiol Dis. 2008; 32:176–182. [PubMed: 18678257]

8. Kellinghaus C, Moddel G, Shigeto H, et al. Dissociation between in vitro and in vivo epileptogenicity in a rat model of cortical dysplasia. Epileptic Disord. 2007; 9:11–19. [PubMed: 17307707]

9. Scantlebury MH, Gibbs SA, Foadjo B, et al. Febrile seizures in the predisposed brain: a new model of temporal lobe epilepsy. Ann Neurol. 2005; 58:41–49. [PubMed: 15940665]

10. Luhmann HJ, Raabe K, Qu M, Zilles K. Characterization of neuronal migration disorders in neocortical structures: extracellular in vitro recordings. Eur J Neurosci. 1998; 10:3085–3094. [PubMed: 9786203]

11. Luhmann HJ, Karpuk N, Qu M, Zilles K. Characterization of neuronal migration disorders in neocortical structures. II. Intracellular in vitro recordings. J Neurophysiol. 1998; 80:92–102. [PubMed: 9658031]

12. Nabbout R, Dulac O. Epileptic encephalopathies: a brief overview. J Clin Neurophysiol. 2003; 20:393–397. [PubMed: 14734929]

13. Nickels K, Wirrell E. Electrical status epilepticus in sleep. Semin Pediatr Neurol. 2008; 15:50–60. [PubMed: 18555191]

14. Tuchman R. CSWS-related autistic regression versus autistic regression without CSWS. Epilepsia. 2009; 50(Suppl 7):18–20. [PubMed: 19682044]

15. Rossi PG, Parmeggiani A, Posar A, et al. Landau-Kleffner syndrome (LKS): long-term follow-up and links with electrical status epilepticus during sleep (ESES). Brain Dev. 1999; 21:90–98. [PubMed: 10206525]

16. Sun QQ, Huguenard JR, Prince DA. REORGANIZATION OF BARREL CIRCUITS LEADS TO THALAMICALLY-EVOKED CORTICAL EPILEPTIFORM ACTIVITY. Thalamus Relat Syst. 2005; 3:261–273. [PubMed: 18185849]

17. Wu C, Wais M, Sheppy E, et al. A glue-based, screw-free method for implantation of intra-cranial electrodes in young mice. J Neurosci Methods. 2008; 171:126–131. [PubMed: 18420280]

18. Lin-Michell E, Chweh AY, Swinyard EA. Effect of ethosuximide alone and in combination with gamma-aminobutyric acid receptor agonists on brain gamma-aminobutyric acid concentration, anticonvulsant activity and neurotoxicity in mice. J Pharmacol Exp Ther. 1986; 237:486–489. [PubMed: 3009789]

19. Welker E, Van der LH. Quantitative correlation between barrel-field size and the sensory innervation of the whiskerpad: a comparative study in six strains of mice bred for different patterns of mystacial vibrissae. J Neurosci. 1986; 6:3355–3373. [PubMed: 3772437]

20. Pinault D, Vergnes M, Marescaux C. Medium-voltage 5–9-Hz oscillations give rise to spike-and-wave discharges in a genetic model of absence epilepsy: in vivo dual extracellular recording of thalamic relay and reticular neurons. Neuroscience. 2001; 105:181–201. [PubMed: 11483311]

21. Qiao XX, Noebels JL. Genetic and phenotypic heterogeneity of inherited spike-wave epilepsy: two mutant gene loci with independent cerebral excitability defects. Brain Res. 1991; 555:43–50. [PubMed: 1933329]

22. Silver, LM. Mouse genetics: concepts and applications. New York: Oxford University Press; 1995.

23. Leresche N, Parri HR, Erdemli G, et al. On the action of the anti-absence drug ethosuximide in the rat and cat thalamus. J Neurosci. 1998; 18:4842–4853. [PubMed: 9634550]
24. Coulter DA, Huguenard JR, Prince DA. Characterization of ethosuximide reduction of low-threshold calcium current in thalamic neurons. Ann Neurol. 1989; 25:582–593. [PubMed: 2545161]
25. Beenhakker MP, Huguenard JR. Neurons that fire together also conspire together: is normal sleep circuitry hijacked to generate epilepsy? Neuron. 2009; 62:612–632. [PubMed: 19524522]
26. McCormick DA, Contreras D. On the cellular and network bases of epileptic seizures. Annu Rev Physiol. 2001; 63:815–846. [PubMed: 11181977]
27. Steriade M. Neuronal substrates of spike-wave seizures and hypsarrhythmia in corticothalamic systems. Adv Neurol. 2006; 97:149–154. [PubMed: 16383124]
28. Zhao S, Ting JT, Atallah HE, et al. Cell type-specific channelrhodopsin-2 transgenic mice for optogenetic dissection of neural circuitry function. Nat Methods. 2011; 8:745–752. [PubMed: 21985008]
29. Barneoud P, Gyger M, Andres F, et al. Vibrissa-related behavior in mice: transient effect of ablation of the barrel cortex. Behav Brain Res. 1991; 44:87–99. [PubMed: 1910574]
30. Schwartzkroin, PA., editor. Encyclopedia of Basic Epilepsy Research. Oxford: Academic Press; Cortical malformations as a cause for epileptiform activity: the freeze lesion model; p. 187-191.
31. Patry G, Lyagoubi S, Tassinari CA. Subclinical “electrical status epilepticus” induced by sleep in children. A clinical and electroencephalographic study of six cases. Arch Neurol. 1971; 24:242–252. [PubMed: 5101616]
32. Hagemann G, Kluska MM, Redecker C, et al. Distribution of glutamate receptor subunits in experimentally induced cortical malformations. Neuroscience. 2003; 117:991–1002. [PubMed: 12654351]
33. Jacobs KM, Gutnick MJ, Prince DA. Hyperexcitability in a model of cortical maldevelopment. Cereb Cortex. 1996; 6:514–523. [PubMed: 8670677]
34. Jacobs KM, Mogensen M, Warren E, Prince DA. Experimental microgyri disrupt the barrel field pattern in rat somatosensory cortex. Cereb Cortex. 1999; 9:733–744. [PubMed: 10554996]
35. Kharazia VN, Jacobs KM, Prince DA. Light microscopic study of GluR1 and calbindin expression in interneurons of neocortical microgyral malformations. Neuroscience. 2003; 120:207–218. [PubMed: 12849753]
36. Schmidt S, Bruehl C, Hagemann G, et al. Impairment of functional inhibition in the contralateral cortex following perinatally acquired malformations in rats. Exp Neurol. 2006; 201:270–274. [PubMed: 16750529]
37. Shimizu-Okabe C, Okabe A, Kilb W, et al. Changes in the expression of cation-Cl-cotransporters, NKCC1 and KCC2, during cortical malformation induced by neonatal freeze-lesion. Neurosci Res. 2007; 59:288–295. [PubMed: 17904674]
38. Zhou FW, Chen HX, Roper SN. Balance of inhibitory and excitatory synaptic activity is altered in fast-spiking interneurons in experimental cortical dysplasia. J Neurophysiol. 2009; 102:2514–2525. [PubMed: 19692507]
39. Zhou FW, Roper SN. Densities of glutamatergic and GABAergic presynaptic terminals are altered in experimental cortical dysplasia. Epilepsia. 2010; 51:1468–1476. [PubMed: 20477846]
40. Redecker C, Luhmann HJ, Hagemann G, et al. Differential downregulation of GABAA receptor subunits in widespread brain regions in the freeze-lesion model of focal cortical malformations. J Neurosci. 2000; 20:5045–5053. [PubMed: 10864962]
41. Matejovska I, Veliskova J, Velisek L. Bicuculline-induced rhythmic EEG episodes: gender differences and the effects of ethosuximide and baclofen treatment. Epilepsia. 1998; 39:1243–1252. [PubMed: 9860058]
42. Zhou FW, Rani A, Martinez-Diaz H, et al. Altered behavior in experimental cortical dysplasia. Epilepsia. 2011; 52:2293–2303. [PubMed: 21933180]

Key Point Box

- For the first time, we report that a unilateral single neonatal freeze lesion in the somatosensory cortex induces spontaneous epileptic seizure events in adult mice.
- The epileptic discharge pattern closely resembled the pattern of continuous spike-waves during slow-wave sleep (CSWS) and ESES and are more frequent in females.
- CSWS were synchronized at around 10 Hz between different regions and were suppressed by ethosuximide and bilateral optogenetic cortical activation of GABAergic neurons.

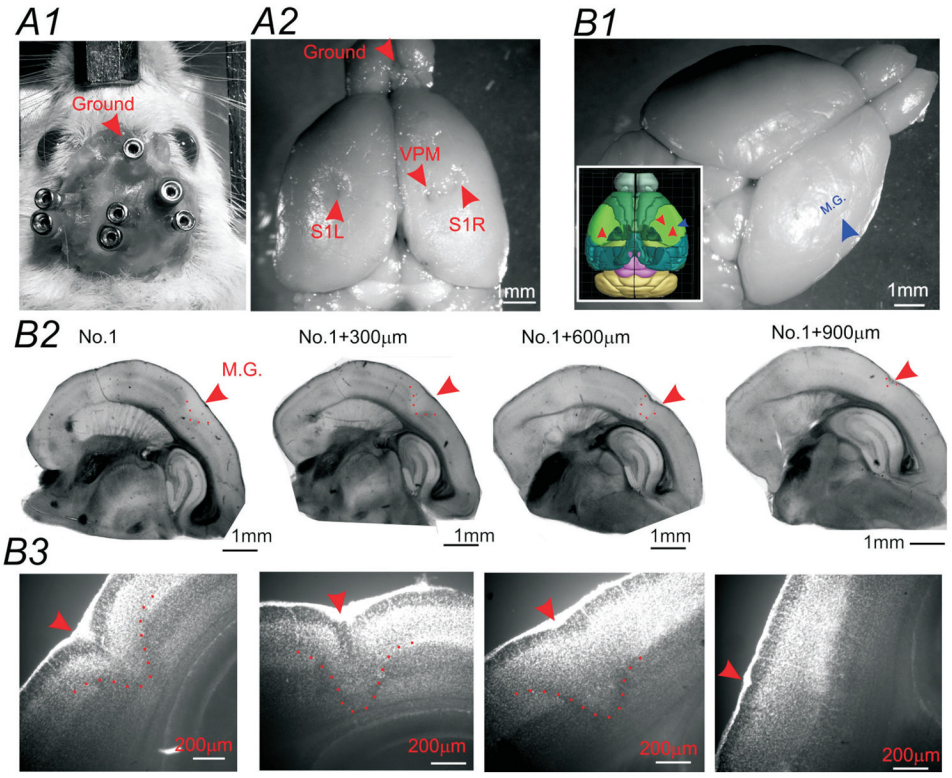

Figure 1.

EEG recording montage and histological verification of cortical malformations in SFLS1R animals. (**A)** Photomicrograph of the screw-free EEG electrodes placement in an anesthetized mouse. In this animal, three bipolar EEG electrodes, with connecting female pins were implanted into S1R, S1L and VPM, with a ground electrode implanted near the center of the olfactory bulb area (A1). Whole brain image indicating the histological verification of the electrode track positions (A2). ***(B)*** In SFLS1R animals, the microgyrus (M.G.) was visible on the surface of the brain. Sagittal sections from the same brain indicating the location of the M.G. (red arrow and dotted line) in reference to other brain structures (B2). Higher magnification of the same sections shown in B2 demonstrates the laminar disruption of the S1 cortex induced by the M.G. (red arrows and dotted line, DAPI stain) (B3).

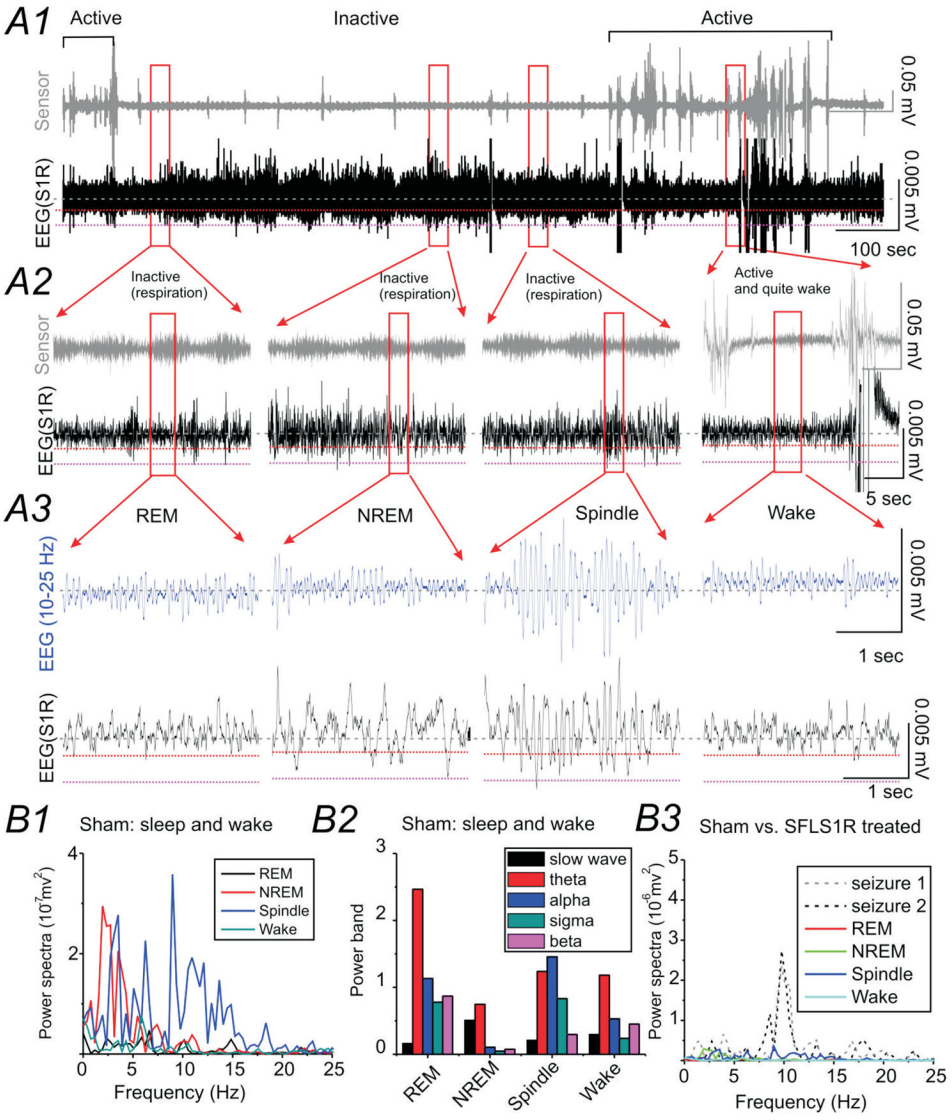

Figure 2. Normal EEG sleep waveforms in sham-treated animals

(A) Representative EEG recording during normal sleep from the right S1 cortex (S1R) of a sham-treated mouse (A1). The top trace (grey) is a simultaneous recording from a piezo-electric floor sensor used to detect animal movement and respiration. The bottom trace (black) is the cortical S1R EEG recording. The red dotted line within the EEG recording shows a threshold voltage of 0.002 mV from baseline and the black dotted line marks voltage-value of 0.005 mV. EEG from selected areas (red square) are expanded in A2 and further expanded in A3 to demonstrate the spectro-temporal profile of the slow-wave, REM sleep and spindle activity observed during sleep and during quiet wake. A band-pass (10–25 Hz) filtered EEG signal (blue trace) is also shown to enhance the view of spindle activity. **(B)** Power analysis of EEG signals during sleep and wake. B1) Power spectrum analysis for each of the traces shown above. B2) Power-band data for different sleep and wake stages shown above. B3) The scale of the power-spectra for different sleep stages was set the same

as in Figure 3B1 for comparison between SFLS1R-induced ictal-spike activities and sleep in this sham-treated animal.

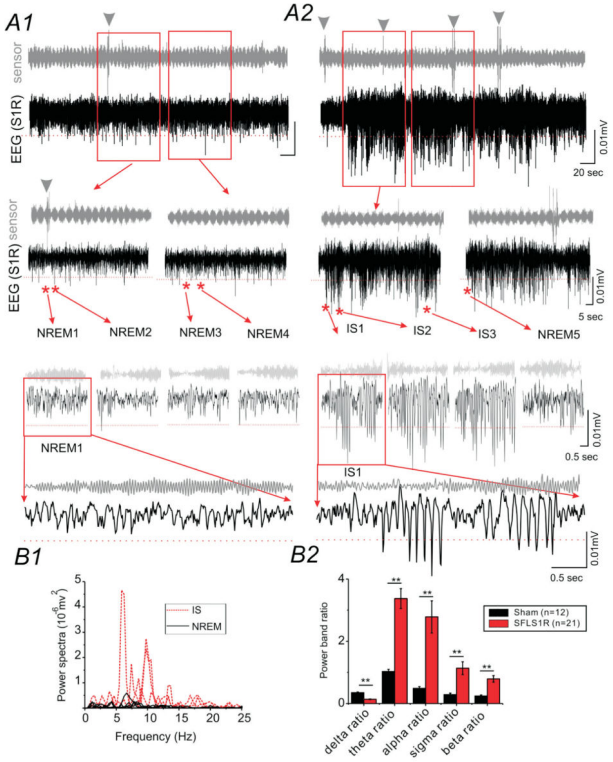

Figure 3. SFLS1R-induced electrographic seizures

(A) Representative EEG recording from the right S1 cortex of an SFLS1R mouse which contains both normal sleep (A1) and the ictal (A2) state. The top trace (grey) is a simultaneous recording from a piezo-electric floor sensor. The bottom trace (black) is the cortical S1R EEG recording. The EEG traces from the selected (red squares) areas are further expanded to demonstrate the spectro-temporal profile of non-rapid eye movement (NREM) sleep versus ictal-spike (IS) activity. The red dotted line within EEG recording shows a threshold voltage of 0.005 mV from baseline The power spectrum derived from the representative NREM sleep (solid black lines) and IS activity (dotted red lines) are shown in B1. **(B)** Representative individual power-spectrum plot for traces shown above (B1) and quantitative power-band analysis of ictal-spikes (SFLS1R animals, n=21) vs. NREM sleep in selected cohort of animals (sham animals, n=12, **: $p<0.01$).

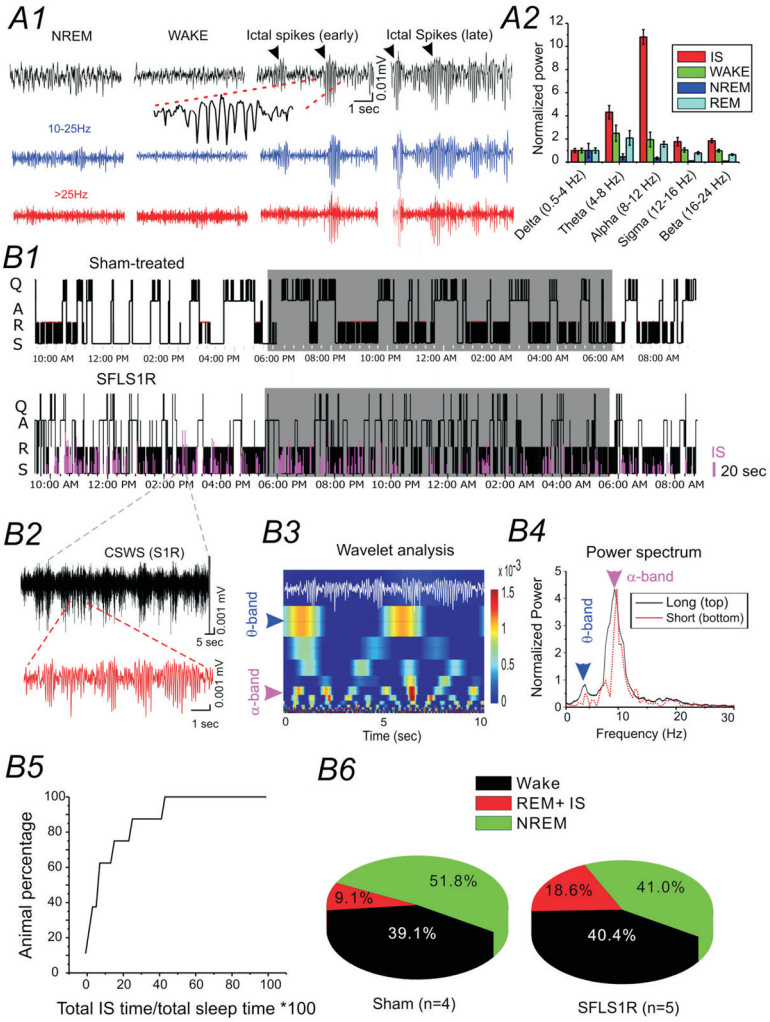

Figure 4. Ictal-spike activity across sleep-wake cycles

(A) Comparison of IS activity with EEG from different vigilance states. A1: Original and band-pass filtered EEG activity. A2: Power-band analysis of different EEG states and IS. **(B)** IS activity and sleep-wake cycle. B1) Hypnogram of a sham (top) and SFLS1R mouse (bottom). IS activity is plotted in relationship to the sleep-wake cycle. Shaded area represents the dark cycle. Q: Quiet wake; A: active wake; N: NREM sleep; R: REM sleep. B2) a segment of CSWS activity (black) composed of repetitive ictal-spikes (red). B3) Wavelet analysis indicating that IS segments are composed of distinct spectral peaks across the α and θ band. B4) Power-spectrum analysis of CSWS activity indicating a dominant peak in the α band and a secondary peak in the θ band for both the long (black solid trace) and short (red dotted trace) EEG samples shown in B2. B5) Cumulative plot of total IS time/ total sleep time in 5 S1RSFL mice exhibiting IS activity. B6) The distribution of wake, NREM sleep and REM sleep state and IS activities in sham-treated vs. S1RSFL mice.

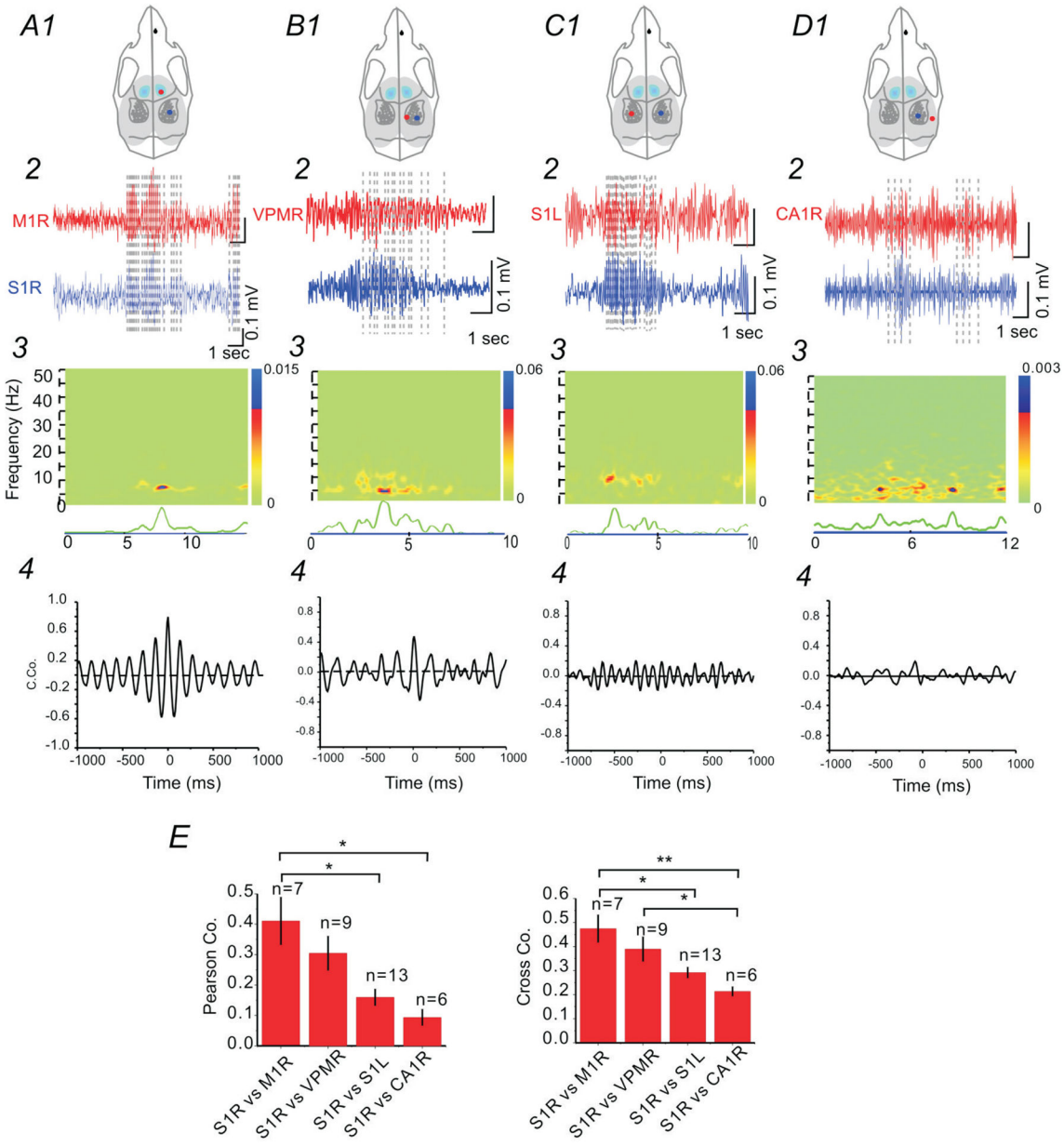

Figure 5. Cross-correlation analysis of ictal-spikes between different brain regions

Comparison of IS activity from ipsilateral S1 and M1 regions indicated the highest degree of synchronization **(A)**, compared with other regions (S1R vs. ipsilateral VPM, **B**; S1R vs. contralateral S1, **C**; and S1R vs. ipsilateral hippocampus, **D**). Top (1): drawings of skull showing the location of the recording electrodes in relationship to barrel field. 2: Comparison of EEG recordings from different brain regions. 3: Spectral coherence plot indicating the degree of signal coherence across both frequency and time. 4: Cross-correlation between the two selected EEG segments. **(E)** Group data showing two different cross-correlation analyses (Pearson vs. Cross-correlation) from simultaneous recordings (n=6–13 per group, *: $p<0.05$; **: $p<0.01$).

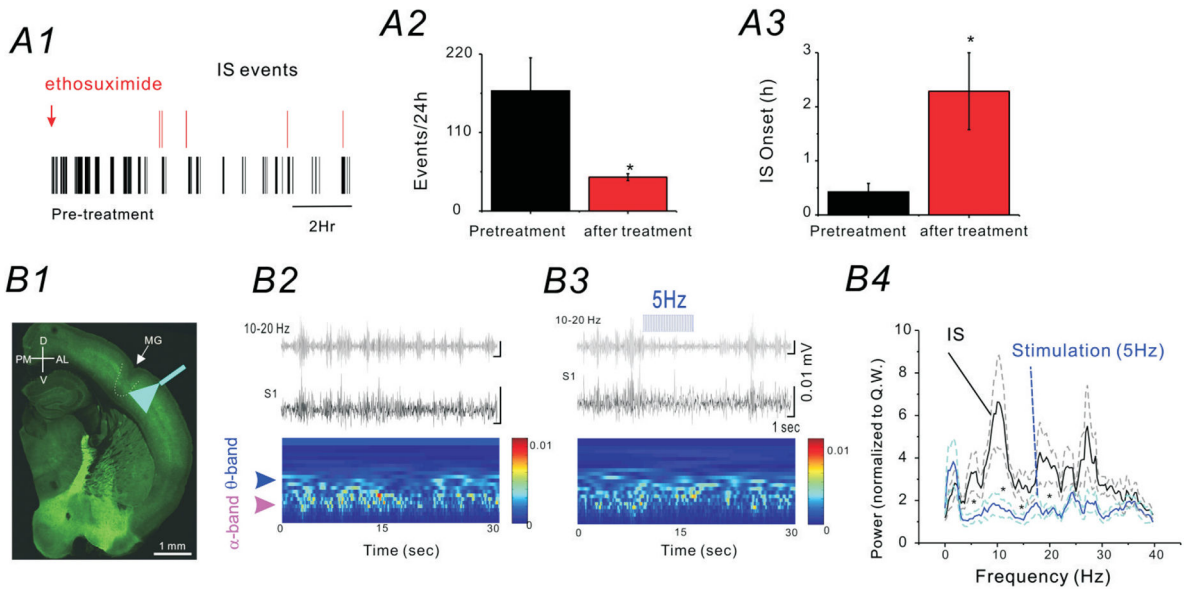

Figure 6. CSWS is modulated by ethosuximide and bilateral optogenetic cortical activation of GABAergic neurons

(A) Effects of ethosuximide administration (2 mg/0.5 ml distilled water via i.p. bolus injection) on CSWS activity in SFLS1R mice. A1) Representative raster plot of each IS event detected during a 24 h period, prior to (black) and after (red) ethosuximide administration. A2) The total number of IS events recorded in a 24h period before (black) and after (red) ethosuximide administration (n=6, *p<0.05). A3) The onset of the first IS event detected after time 0 (sham-injection or ethosuximide injection, n=6, *p<0.05). **(B)** The effects of optogenetic activation of GABAergic neurons on CSWS activity in SFLS1R mice. B1) A thalamocortical brain slice from a SFLS1R/VGAT-ChR2 mouse showing the site of the microgyrus (MG) and the location of the fiber-optic implant. The green-fluorescence is derived from the endogenous fusion protein-YFP that was fused with the ChR2 gene. B2) Top: EEG recordings (black trace) of ictal-spikes and a 10–20 Hz band-pass filtered trace (grey) in S1R. Bottom: wavelet analysis showing the two characteristic power peaks in the α and θ band. B3) Top: Once the IS activity was detected, a 5 Hz optogenetic laser stimulation was applied in the adjacent ipsilateral (not shown) or contralateral (B3) S1 region. Bottom: α and θ band power was reduced when the 5 Hz optogenetic stimulation was applied. B4) Power-spectrum analysis of ictal-spikes with (blue) or without (black) 5 Hz optogenetic stimulation. The dotted lines represent the S.E. of the mean. n=6 mice, *: p<0.05.

Table 1

Behavior analysis in SFLS1R mice w/CSWS seizures vs. SFLS1R mice w/o CSWS seizures.

Tests	SFLS1R-w/o	SFLS1R-w/CSWS	P value
OF/Center time (min)	1.1 ± 0.43 N = 11	0.80 ± 0.50 N=20	0.02
OF/active counts	1555 ± 253 N = 10	1401 ± 262 N = 20	0.002
SI/time with stranger (min)	3.7 ± 1.4 N = 11	4.6 ± 2.2 N=13	0.02
NOR/novel obj. (sec)	11.8 ± 11.4 N = 6	23.3 ± 18.0 N = 13	0.02
NOR/Familiar obj (sec).	5.0 ± 4.0 N = 6	11.0 ± 10.4 N = 13	0.11
Gap crossing distance (cm)	7.5±0.5 N=5	6.8±0.7 N=4	0.36

OF/Center time (min): average activity during 10 min OF testing period. SI/time with stranger: average time spent with stranger mouse during a 10 min SI test. NOR/novel obj.: average time investigating a novel object versus a familiar object during a 5 min NOR test, presented as the total time sniffing each object. All values represent average ± S.E.M.